Monografías de la Real Academia de Ciencias de Zaragoza **31**, 121–135, (2009).

Application of numerical models to real problems: Simulation of flood events with ecological interest in the Ebro River

M. González-Sanchís*, J. Murillo+, D. López-Barrera+,
B. Latorre+, F. Comín* and P. García-Navarro+

*IPE-CSIC

+Fluid Mechanics. CPS. University of Zaragoza

Abstract

The application of a finite volume numerical scheme for 2D shallow-water equations to flood events in the Ebro River is presented. The area of interest is a Natural Reserve playing an important role in protecting human settlements from flooding events and developing important biological functions like water quality improvement, wildlife refuge, landscape heterogeneity, etc. The hydraulic model used is based in the 2D transient shallow water equations on irregular bed solved with an explicit finite volume upwind scheme able to compute flow advance over dry bed. This model has been calibrated during the last years in a wide range of real and academic cases giving an efficient result. This study involves the reliable simulation of, not only the flood event itself but the drying processes. It is necessary to remark the importance of the correct characterisation of the roughness coefficient and the topography. The former is estimated from a previous classification of structurally homogeneous habitats and the latter is defined by merging the DTM data with the field-measured ones. The calibration of the suitability of the model to solve this problem is based on different sets of field measurements: flooded area and water levels measured during a flood event and time series of point-wise measurements of water-depth and velocity during different situations along the year. Hydrological connectivity is highly related to the exchange processes of nutrients and particulate matter between the river and the floodplain. It represents an indicator of the dynamics of the ecological processes in the floodplain and, consequently, is a key factor to be considered for the restoration of degraded habitats of floodplains. The model presented is a tool that helps to analyse the surface processes involved.

Keywords: Hydrological connectivity, Unsteady surface flow, wetting/drying, Finite volume, Shallow-water.

1 Introduction

Flooding facilitates the exchange of materials and energy between rivers and their floodplains ([4], [17], [1]). Hydrological connectivity is the driving force of the lateral exchange processes, both via surface flow and via groundwater pathways ([19]). In the past century, flow regulation has reduced or eliminated hydrological and ecological interactions between many rivers and their floodplains ([16]). To interpret and predict the changes in ecological characteristics of riparian wetlands across multiple spatial and temporal scales, it is essential to know the hydrological relationships between the river and its floodplain. On shorter time scales (days to months), the hydrological connectivity between landscape elements varies in response to the flow pulse, that is, water level fluctuations that are well below bankfull ([19]). On an annual or supra-annual scale, erosive floods are capable of creating and maintaining habitat patches at a variety of successional stages, which, in turn, determine the overall permeability and complexity of the landscape matrix ([18], [15]). It is clear that hydrological connectivity is a key factor to be considered in hydrological restoration, but floodplain topography is an important consideration in the restoration of lowland rivers ([2]). In this context, the numerical simulation of the overland water flow is used as a tool to know the hydrological floodplain dynamics and to predict the hydrological dynamic when a terrain change happens, like gravel deposition, dyke broke, dyke construction, etc.

In recent years, finite volume techniques based on upwind and TVD (Total Variation Diminishing) numerical schemes have been successfully applied in Fluid Dynamics to simulate one and two-dimensional free surface flows ([8], [12]). In particular, one- and two-dimensional numerical models have been developed as tools to design and manage river basin systems. In river modelling, the flow can be assumed to be governed by the Shallow Water equations ([7]) where the bottom friction and bed level irregularities have been shown to influence not only flood waves behaviour but also numerical methods performance drastically. The hydraulic model is based on the shallow water flow equations in two dimensions and is used to simulate unsteady flows in complex geometries. A cell centered finite volume method based on Roe's approximate Riemann solver ([5], [6]) across the edges of both structured and unstructured cells is used. The discretization of the bed slope source terms is done following an upwind approach ([13]). In some applications a problem arises when the flow propagates over adverse dry bed slopes, so a special procedure has been introduced to model the advancing front. It has been shown that this modification reproduces exactly the steady state of still water in configurations with strong variations in bed slope and contour and provides a fully conservative solution in all cases ([14], [10]). The scheme is able to handle complex flow domains as will be shown in the simulations corresponding to the field test cases that are going to be presented.

2 Description of the study area

The study area is in the Middle Ebro River in northeast Spain and comprises a watershed area of 85362 km^2. The Ebro River, 910 km long, is the largest river in Spain. It has an annual discharge into the Mediterranean Sea of 18138 hm^3/y and remains geomorphologically active despite the presence of 170 dams and reservoirs on the river and its tributaries. The reach of the Ebro River in the study area forms a meander (211 ha, river wide: 110 m with one island and an oxbow lake) situated downstream Zaragoza city and included in the Natural Reserve "Los Galachos" (see Fig.1). The discharge, averaged over the years 1927 to 2003, within this reach is 230 m^3/s and the surface elevation ranges from 175 m asl at the river channel to 185 m asl at the base of the old river terrace. The flooded area by the 10-yr return period flood (3000 m^3/s, 1927–2003) is 211 ha, although only about 14% of the area is flooded by a river discharge of 1000 m^3/s (0.37 y return period, 1927–2003), and only 4% is flooded by a river discharge of 600 m^3/s (0.14 y return period, 1927–2003). The oxbow lake is connected with the river when the discharge is 1000 m^3/s, it occurs 1–3 times per year. During the last century, the number and extent of permanent water bodies has declined considerably.

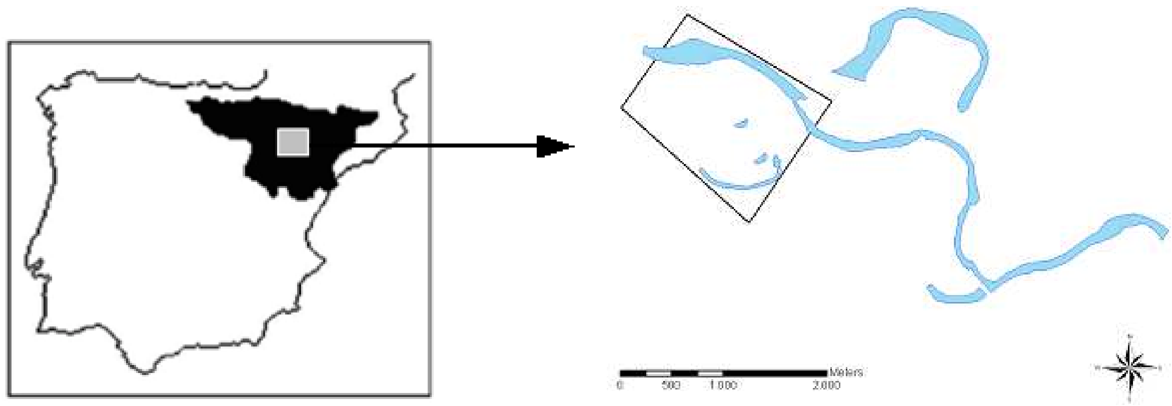

Figure 1: Area of study.

2.1 Topography

The Digital Terrain Model (DTM) used in this paper was provided by the Ebro River Basin Administration (www.chebro.es) as a support to the research project. It had been obtained using the Laser light detection and ranging (LIDAR) technology. The DTM has 0.15 m accuracy and 1m resolution that supplies good quality information about all the surface not covered by water. The main channel shape has been characterised with an in-situ bathymetry using a depth portable sounder. A bed elevation map of the full domain was thereafter produced by interpolating these measured values with the DTM data. For the terrain discretization we use the ArcGis software (resample tool), by transforming the network from 1 m resolution to 5 m.

2.2 Roughness

The floodplain roughness has been characterised dividing the floodplain in a set of habitats of homogeneous structure. The roughness coefficient has been assigned to each habitat according to the recommendations found in the specialized bibliography .

3 Simulation model

The water flow, in some circumstances, can be modelled according to the shallow water model [10]). This is a system of equations derived from the Navier-Stokes equations for incompressible flow by averaging in the water depth ([7]). It can be written as:

$$\frac{\partial \mathbf{U}}{\partial t} + \frac{\partial \mathbf{F(U)}}{\partial x} + \frac{\partial \mathbf{G(U)}}{\partial y} = \mathbf{S}(x, y, \mathbf{U}), \tag{1}$$

$$\begin{aligned} \mathbf{U} &= \begin{pmatrix} h \\ hu \\ hv \end{pmatrix}, \qquad \mathbf{F} = \begin{pmatrix} hu \\ hu^2 + \frac{1}{2}gh^2 \\ huv \end{pmatrix}, \\ \mathbf{G} &= \begin{pmatrix} hv \\ huv \\ hv^2 + \frac{1}{2}gh^2 \end{pmatrix}, \quad \mathbf{S} = \begin{pmatrix} 0 \\ gh(S_{0x} - S_{fx}) \\ gh(S_{0y} - S_{fy}) \end{pmatrix}, \end{aligned} \tag{2}$$

where h is the water depth, u is the x-component of the depth averaged flow velocity, v is the y-component of the depth averaged flow velocity, g is the acceleration of the gravity, S_{0x} and S_{0y} are the bed slopes in the x and y directions respectively, and S_{fx} and S_{fy} are the hydraulic energy slopes also in the x and y directions:

$$S_{0x} = -\frac{\partial z}{\partial x}, \quad S_{0y} = -\frac{\partial z}{\partial y}, \tag{3}$$

$$S_{fx} = \frac{n^2 u \sqrt{u^2 + v^2}}{h^{4/3}}, \quad S_{fy} = \frac{n^2 v \sqrt{u^2 + v^2}}{h^{4/3}}, \tag{4}$$

where the energy slopes have been modelled by means of the semi-empirical Manning friction law [7]. The functions (3) and (4) determine the source terms in the shallow water system of equations (1). The system is hyperbolic and will be solved by means of a finite volume method so that it is convenient to reformulate it as:

$$\frac{\partial \mathbf{U}}{\partial t} + \overrightarrow{\nabla} \mathbf{E(U)} = \mathbf{S}(x, y, \mathbf{U}), \tag{5}$$

where the flux $\mathbf{E} = [\mathbf{F}, \mathbf{G}]$ is defined in order to highlight the conservative law structure of the system in the homogeneous case. The integration of (5) within a volume Ω, gives:

$$\frac{\partial}{\partial t}\int_{\Omega} \mathbf{U} d\Omega + \int_{\Omega} (\vec{\nabla}\mathbf{E}) d\Omega = \int_{\Omega} \mathbf{S} d\Omega. \tag{6}$$

Using the Gauss theorem in the second term:

$$\frac{\partial}{\partial t}\int_{\Omega} \mathbf{U} d\Omega + \oint_{\delta\Omega} (\mathbf{E}\cdot\mathbf{n}) d\Omega = \int_{\Omega} \mathbf{S} d\Omega, \tag{7}$$

where $\delta\Omega$ represents the surface limiting the volume Ω and $\mathbf{n}$ the outward unit normal vector. It is useful to define the Jacobian matrix $\mathbf{J}_n$ of the normal flux $(\mathbf{E}\cdot\mathbf{n})$ of our hyperbolic system of equations, so that:

$$\mathbf{J}_n = \frac{\partial(\mathbf{E}\cdot\mathbf{n})}{\partial\mathbf{U}} = \frac{\partial\mathbf{F}}{\partial\mathbf{U}} n_x + \frac{\partial\mathbf{G}}{\partial\mathbf{U}} n_y, \tag{8}$$

with components:

$$\mathbf{J}_n = \begin{pmatrix} 0 & n_x & n_y \\ (gh-u^2)n_x - uvn_y & vn_y + 2un_x & vn_y \\ (gh-v^2)n_y - uvn_x & vn_x & un_x + 2vn_y \end{pmatrix} \tag{9}$$

The eigenvalues of $\mathbf{J_n}$ represent the characteristic celerities of the information relevant in our model:

$$\lambda^1 = \mathbf{u}\cdot\mathbf{n} + c, \quad \lambda^2 = \mathbf{u}\cdot\mathbf{n}, \quad \lambda^3 = \mathbf{u}\cdot\mathbf{n} - c, \tag{10}$$

where $\mathbf{u} = (u, v)$, $\mathbf{n} = (n_x, n_y)$ and $c = \sqrt{gh}$ is the celerity of the small amplitude surface waves. The eigenvectors of the normal Jacobian are:

$$\mathbf{e}^1 = \begin{pmatrix} 1 \\ u + cn_x \\ v + cn_y \end{pmatrix}, \quad \mathbf{e}^2 = \begin{pmatrix} 0 \\ -cn_y \\ cn_x \end{pmatrix}, \quad \mathbf{e}^3 = \begin{pmatrix} 1 \\ u - cn_x \\ v - cn_y \end{pmatrix}. \tag{11}$$

Matrices $\mathbf{P}$ and $\mathbf{P}^{-1}$ can be built from the eigenvectors so that they diagonalize $\mathbf{J}_n$:

$$\mathbf{J}_n = \mathbf{P}\Lambda\mathbf{P}^{-1}, \quad \Lambda = \mathrm{diag}(\lambda^1, \lambda^2, \lambda^3). \tag{12}$$

$$\mathbf{P} = \begin{pmatrix} 1 & 0 & 1 \\ u + cn_x & -cn_y & u - cn_x \\ v + cn_y & cn_x & v - cn_y \end{pmatrix}, \mathbf{P}^{-1} = \frac{1}{2c}\begin{pmatrix} -\mathbf{u}\cdot\mathbf{n} + c & n_x & n_y \\ 2(un_y - vn_x) & -2n_y & 2n_x \\ \mathbf{u}\cdot\mathbf{n} + c & -n_x & -n_y \end{pmatrix}. \tag{13}$$

This is the basis of the finite volume method. Next, the discretization technique is outlined.

4 Numerical Method

The method used to solve the system of shallow water equations (1) will follow the previous works [8] and [10]). This is a cell centered finite volume method formulated so that the functions are piecewise constant per grid cell or first order in space ([3]). The computational domain is discretized in either triangular or quadrilateral cells that can be aligned or not with the coordinate axis. So the method is designed to work on both structured and unstructured grids. A discrete approximation is applied to (7) all over the mesh cells Ω_i at a given time. The integration along one time step can be interpreted as the time variation of the integral over the cell area and the surface integrals represent the total flow across the boundaries. Calling U_i the uniform value of the conserved variables in volume/grid cell Ω_i at a given time, (7) can be rewritten:

$$\frac{\delta \mathbf{U}_i}{\delta t} A_i + \oint_{\partial \Omega_i} (\mathbf{E} \cdot \mathbf{n}) dS = \int_{\Omega_i} \mathbf{S} d\Omega, \tag{14}$$

where A_i is the area of cell Ω_i. The grid is assumed fixed in time and the surface/contour integral is approximated by a sum over the cell edges. The normal flux is evaluated following an upwind flux difference splitting technique ([3]) as follows:

$$\oint_{\partial \Omega} (\mathbf{E} \cdot \mathbf{n}) dS \approx \sum_{k=1}^{NE} (\delta \mathbf{E}_k \cdot \mathbf{n}_k) s_k, \tag{15}$$

and subindex k labels the edges of the cell Ω_i, NE represents the number of cell edges (4 if rectangular and 3 when triangular). The unit vector $\mathbf{n}_k$ is the ourward normal to cell edge k, s_k being the length of that side and $\delta \mathbf{E}_k \cdot \mathbf{n}_k$ is the normal flux difference.
Upwind schemes are based on the idea of discretizing the flux spatial derivatives according to the propagation of the relevant physical information ([9]). When dealing with conservation laws with source terms, the later must be discretized in the same form as the flux derivative terms [20], [8]. The discrete evaluation of flow and source terms at the same local state is important in many cases to achieve discrete equilibrium at steady state [13], [10] and therefore to make sure that the numerical solution has the best properties during transients.

The existence and the properties of the Jacobian matrix allow a local linearization [5], of the form:

$$\delta(\mathbf{E} \cdot \mathbf{n}) = \widetilde{\mathbf{J}}_{RL} \delta \mathbf{U}, \tag{16}$$

with $\delta \mathbf{U} = \mathbf{U}_R - \mathbf{U}_L$ calling Ω_L the left cell to a given edge and Ω_R the right cell (the normal vector to the edge is assumed to point from L to R), as sketched in figure 2.

This linearization can be used to build the discretization of the normal fluxes across the computational cell edges. The local definition of an approximate Jacobian matrix, $\widetilde{\mathbf{J}}_{RL}$

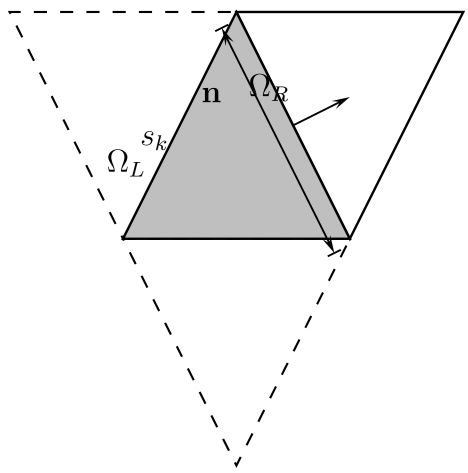

Figure 2: Elements in a structured triangular grid.

is required. According to Roe [5], matrix $\widetilde{\mathbf{J}}_{RL}$ has the same form as $\mathbf{J}_n$ but is evaluated at an average state given by the quantities $\widetilde{\mathbf{u}} = (\widetilde{u}, \widetilde{v})$ and $\widetilde{c}$, which must be derived from the matrix properties:

1. $\widetilde{\mathbf{J}}_{RL} = \widetilde{\mathbf{J}}_{RL}(\mathbf{U}_R, \mathbf{U}_L)$
2. $(\mathbf{E} \cdot \mathbf{n})_R - (\mathbf{E} \cdot \mathbf{n})_L = \widetilde{\mathbf{J}}_{RL}(\mathbf{U}_R - \mathbf{U}_L)$
3. $\widetilde{\mathbf{J}}_{RL} = \widetilde{\mathbf{J}}_{RL}(\mathbf{U}_R) = \widetilde{\mathbf{J}}_{RL}(\mathbf{U}_L)$ if $\mathbf{U}_R = \mathbf{U}_L$

Therefore,

$$\widetilde{\mathbf{J}}_{RL} = \begin{pmatrix} 0 & n_x & n_y \\ \widetilde{c}^2 n_x + \widetilde{\mathbf{u}} \cdot \mathbf{n} \widetilde{u} & \widetilde{u} n_x + \widetilde{\mathbf{u}} \cdot \mathbf{n} & \widetilde{u} n_y \\ \widetilde{c}^2 n_y - \widetilde{\mathbf{u}} \cdot \mathbf{n} \widetilde{v} & \widetilde{v} n_x & \widetilde{v} n_y + \widetilde{\mathbf{u}} \cdot \mathbf{n} \end{pmatrix}, \tag{17}$$

where

$$\widetilde{u} = \frac{u_R\sqrt{h_R} + u_L\sqrt{h_L}}{\sqrt{h_R} + \sqrt{h_L}}, \quad \widetilde{v} = \frac{v_R\sqrt{h_R} + v_L\sqrt{h_L}}{\sqrt{h_R} + \sqrt{h_L}}, \quad \widetilde{c} = \sqrt{g\frac{(h_R + h_L)}{2}}. \tag{18}$$

The basic procedure in our method starts by a projection of the vector $\delta\mathbf{U}$, defined at a cell edge, on the basis of eigenvectors:

$$\delta\mathbf{U} = \mathbf{U}_R - \mathbf{U}_L = \sum_{m=1}^{3} \alpha^m \widetilde{\mathbf{e}}^m \tag{19}$$

Where the expressions for the coefficients α^m are:

$$\alpha^{1,3} = \frac{\delta h}{2} \pm \frac{1}{2\widetilde{c}}(\delta\mathbf{q} - \widetilde{\mathbf{u}}\delta h) \cdot \mathbf{n}, \quad \alpha^2 = \frac{1}{\widetilde{c}}(\delta\mathbf{q} - \widetilde{\mathbf{u}}\delta h) \cdot \mathbf{n_T}. \tag{20}$$

Then, at every cell edge, the matrix $\widetilde{\mathbf{J}}_n$ is replaced by its eigenvalues and eigenvectors in the evaluation of the normal flux difference $\widetilde{\mathbf{J}}_{RL}(\mathbf{U}_R - \mathbf{U}_L)$ as follows:

$$\widetilde{\mathbf{J}}_{RL}(\mathbf{U}_R - \mathbf{U}_L) = \sum_{m=1}^{3} \widetilde{\lambda}^m \alpha^m \widetilde{\mathbf{e}}^m. \tag{21}$$

In order to discriminate the sign of the advection in the eigenvalues, the new matrices $\Lambda^{\pm}$ are used, with $\Lambda^{\pm} = (\Lambda \pm |\Lambda|)/2$, therefore,

$$\begin{gathered}\delta(\mathbf{E}\cdot\mathbf{n}) = \widetilde{\mathbf{J}}_{RL}\delta\mathbf{U} = \widetilde{\mathbf{P}}\widetilde{\Lambda}\widetilde{\mathbf{P}}^{-1}\delta\mathbf{U} = \widetilde{\mathbf{P}}(\widetilde{\Lambda}^{+} + \widetilde{\Lambda}^{-})\widetilde{\mathbf{P}}^{-1}\delta\mathbf{U},\\ \delta(\mathbf{E}\cdot\mathbf{n}) = \underbrace{\widetilde{\mathbf{P}}\widetilde{\Lambda}^{-}\widetilde{\mathbf{P}}^{-1}\delta\mathbf{U}}_{\text{Ingoing wave}} + \underbrace{\widetilde{\mathbf{P}}\widetilde{\Lambda}^{+}\widetilde{\mathbf{P}}^{-1}\delta\mathbf{U}}_{\text{Outgoing wave}}.\end{gathered} \tag{22}$$

Only the information carried by the ingoing wave to a cell is used to update the conserved variables. Hence, prior to including the source terms:

$$\frac{\delta\mathbf{U}_i}{\delta t}A_i = -\sum_{k=1}^{NE}\sum_{m=1}^{3}(\widetilde{\lambda}^{m-}\alpha^m\widetilde{\mathbf{e}}^m)_k^n s_k, \tag{23}$$

where $\lambda^- = (\lambda - |\lambda|)/2$.

A specific modification of the Riemann solver is used to overcome the generation of the negative values of depth, that can appear as a consequence of existing wetting/drying fronts. More details of the modification can be found in [10].

The size of the time increment in an explicit scheme such as (15) is limited by numerical stability reasons and controlled by the Courant-Freidrichs-Lewy (CFL) dimensionless number or CFL condition

$$\Delta t = CFL\,\Delta t_{\max}^{CFL}, \quad CFL \leq 1. \tag{24}$$

Where the maximum time step size is chosen among all the $NCELL$ cells:

$$\Delta t_{\max}^{CFL} = \min\left(\Delta t_{\max,i}^{CFL}\right)_{i=1,NCELL}, \tag{25}$$

and

$$\Delta t_{\max,i}^{CFL} = \left(\frac{\min(A_R, A_L)}{\max(\widetilde{\lambda}_k^{m-})s_k}\right)_{k=1,NE}. \tag{26}$$

4.1 Bed slope source terms

The bed slope source terms have been discretized, according to [13], in an upwind form in order to ensure the best discrete balance with the flux terms at least in steady state. At every edge k of every cell Ω_i the source term participates with ingoing contributions built as before:

$$\mathbf{U}_i^* = \mathbf{U}_i^n - \sum_{k=1}^{NE}\sum_{m=1}^{3}((\widetilde{\lambda}^m\alpha^m - \beta^m)\widetilde{\mathbf{e}}^m)_k^n \frac{s_k}{A_i}\Delta t, \tag{27}$$

so that the coefficients β are defined as:

$$\beta^1 = -\frac{\tilde{c}}{2}\delta z \quad \beta^2 = 0 \quad \beta^3 = -\beta^1. \tag{28}$$

Note that the superscript * denotes the value of the updated variable.

4.2 Friction source terms

The friction term, $\mathbf{R}$, representing, as said before, the energy slopes is a vector of components:

$$\mathbf{R} = \begin{pmatrix} 0 \\ -ghS_{fx} \\ -ghS_{fy} \end{pmatrix}. \tag{29}$$

According to Brufau *et al.* ([14]), a pointwise explicit treatment of the friction term produces numerical oscillations when the roughness coefficient is high. Furthermore, near wetting/drying fronts, characterized by small values of water depth, this term dominates over any other influence. To avoid oscillations in the solution, the following condition must be fulfilled:

$$(\mathbf{hu})_i^{n+1} = \begin{cases} \geq 0 & \text{if } (\mathbf{hu})_i^n > 0 \\ \\ \leq 0 & \text{if } (\mathbf{hu})_i^n < 0 \end{cases}, \quad (\mathbf{hv})_i^{n+1} = \begin{cases} \geq 0 & \text{if } (\mathbf{hv})_i^n > 0 \\ \\ \leq 0 & \text{if } (\mathbf{hv})_i^n < 0 \end{cases}. \tag{30}$$

To handle properly the friction term, Brufau ([12]) proposed the following splitting technique:

$$\begin{aligned} (\mathbf{hu})_i^{n+1} &= (\mathbf{hu})_i^* - (gh_iS_{fx})_i^{n+1}\Delta t, \\ (\mathbf{hv})_i^{n+1} &= (\mathbf{hv})_i^* - (gh_iS_{fy})_i^{n+1}\Delta t, \end{aligned} \tag{31}$$

where the values signalled with * are obtained using the updating formula ((27)), assuming that the friction term is not considered in the upwind discretization. Denoting by

$$S_f = \frac{n^2|\mathbf{u}|}{h^{\frac{4}{3}}}, \tag{32}$$

and considering $S_{fi}^{n+1} \cong S_{fi}^{*}$, equation (31) is:

$$\begin{aligned}(\mathbf{hu})_i^{n+1} &= (\mathbf{hu})_i^{*} - (\mathbf{hu})_i^{n+1}(S_f)_i^{*}\Delta t,\\ (\mathbf{hv})_i^{n+1} &= (\mathbf{hv})_i^{*} - (\mathbf{hv})_i^{n+1}(S_f)_i^{*}\Delta t.\end{aligned} \tag{33}$$

Therefore, the stability is unconditionally and the previously calculated values of the variables are updated in a rather straightforward way as follows.

$$(\mathbf{hu})_i^{n+1} = \frac{(\mathbf{hu})_i^{*}}{1 + (S_f)_i^{*} g\Delta t},\ (\mathbf{hv})_i^{n+1} = \frac{(\mathbf{hv})_i^{*}}{1 + (S_f)_i^{*} g\Delta t}. \tag{34}$$

5 Results

To calibrate the model, institutional aerial photographs of previous flooding events and local field measurements of depth water, velocity and flooded area taken by the research team were used.

Nowadays the introduction of digital terrain models (DTM) provides data of great accuracy, but does not furnish any information of the region covered by the water. The definition of the river bottom bed level elevation in 2D simulations is not straightforward as this information is only known at a few cross sections. The interpolation methods based on statistical treatment of the overall information, such as the GIS tools, provide incorrect results when reconstructing the river bed and are therefore unable to recover with accuracy the measured field data. In consequence the numerical results for flood modelling based on the GIS model reconstruction are inaccurate. In a first set of trial simulations, the ArcGis software (topogrid tool) was used to generate the river bed surface from the floodpain surface data and a constant discharge of $500m^3/s$ corresponding to field measured conditions was applied at the inlet boundary with dry bed initial conditions. The computed floodplain was excessively flooded and many habitats were erroneously connected to the river. This is displayed in Fig. 3 where the extension of the computed flooded area has been plotted together with the flooded area measured from differential GPS Topcon® (0.03 m accuracy) when the $500m^3/s$ discharge was flowing at steady state. These results were owing to the main channel interpolation. Then, another interpolation method was developed. It was found that, in order to correctly model the bottom elevation, the relevant information must be taken only from the measured cross sections. Also, it is necessary to take into account the sinuosity described by the main channel and to include this information in the interpolation technique, for instance when defining the distance metrics. Only in this way it is possible to represent correctly the river bed variations. The adequacy of the new interpolation technique is shown in Fig. 4 where both computed and photographed flooded areas match.

The following simulations were performed over the correctly reconstructed river bed. The events simulated corresponded to measured flood events in which the river discharge had increased from a steady value (initial condition) to a larger one (maximum discharge) in a known flooding time. One ordinary event ($783m^3/s$ of maximum discharge) with steady state of $495m^3/s$ as initial condition was the first case. The simulation had six control points where field measurements of water depth were available to calibrate it as shown in Fig. 5. The biggest relative error in water level surface at the control points was -0.48% and all the habitats were found correctly connected to the river. Table 1 displays the values of the measured and computed water levels at three gauging locations labelled A, B and C. The flow velocity was laminar at the floodplain, in agreement with the field measurements. One extraordinary event ($1169m^3/s$ of maximum discharge) with steady state of $495m^3/s$ as initial condition was the first case. The simulation had six control points where field measurements of water depth were available to calibrate it as shown in Fig. 5. The habitats were found correctly connected to the river. Table 2 displays the values of the measured and computed water levels at three gauging locations A, B and C.

Table 1: Upstream discharge Q=783 m^3/s.

Field point	Measured WL	Computed WL	Relative Error
A	181.66 m	181.79 m	-0.07
B	183 m	183 m	0.00
C	181.31 m	181.31 m	0.00

Table 2: Upstream discharge Q=1169 m^3/s.

Fiel point	Measured WL	Computed WL	Relative Error
A	182.63 m	182.56 m	0.04
B	183 m	183 m	0.00
C	181.31 m	181.31 m	0.00

6 Conclusions

The finite volume model based on the unsteady two-dimensional shallow water equations is an excellent tool to know the hydrological connectivity between the river and the floodplain. Simulation can help us to interpret the changes in ecological characteristics and to predict the floodplain hydrodynamic when a terrain modification occurs. The model can be considered useful in ecological restoration studies.

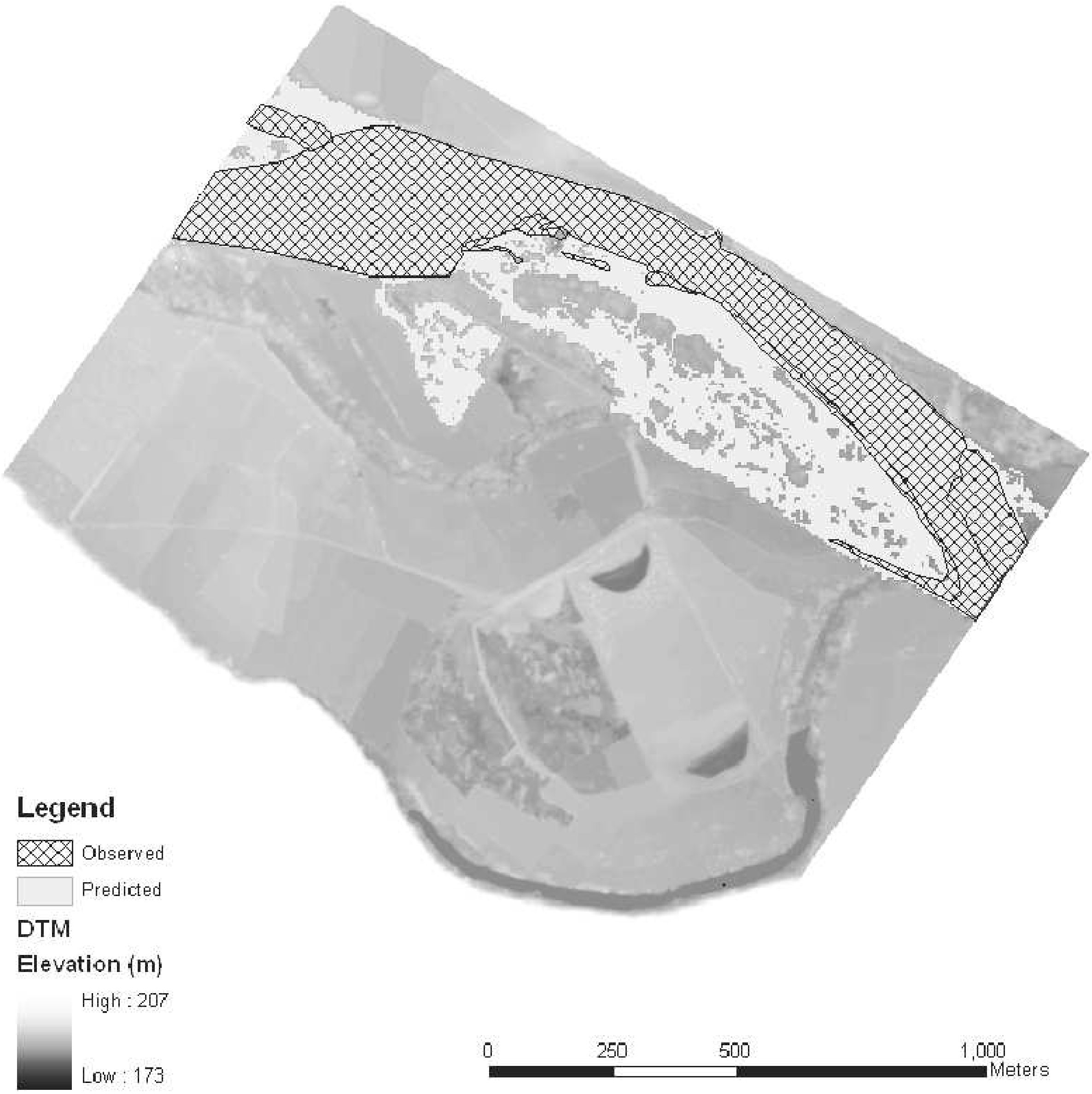

Figure 3: Comparison of the observed flooded area and the computed flooded area using a GIS recontruction of the river bed. Q=500m^3/s.

References

[1] Bayley, P. B.. Understanding large river-floodplain ecosystems. *BioScience* **45**, 153–158, 1995.

[2] Florsheim J.L. and Mount J.F.. Restoration of floodplain topography by sand-splay complex formation in response to intentional levee breaches, Lower Cosumnes River, California. *Geomorphology* **44**. 67–94. 2002

[3] Hirsch,C., Numerical Computation of Internal and External Flows, Vol.2, John Wiley and Sons, 1990.

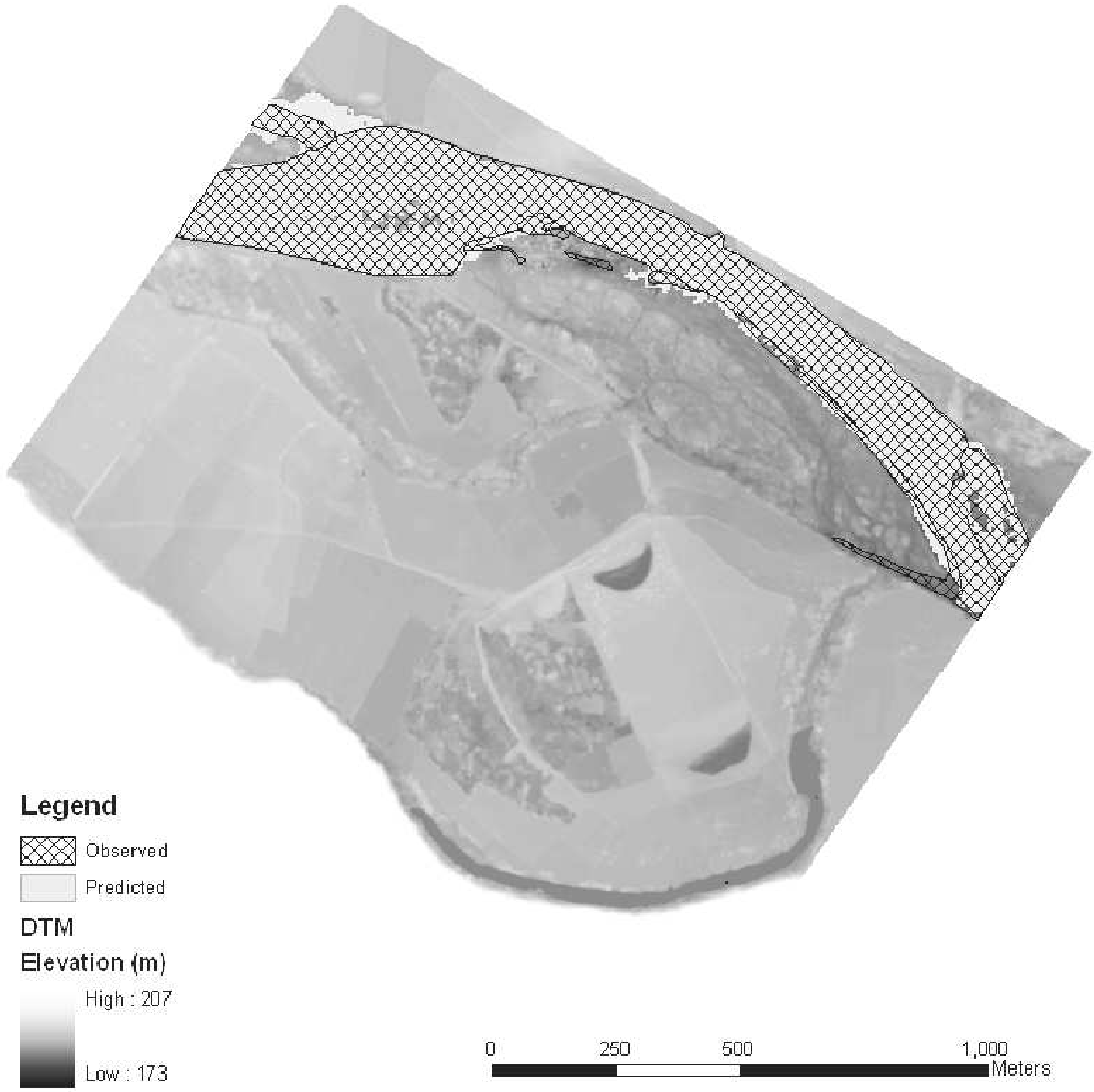

Figure 4: Comparison of the observed flooded area and the computed flooded area using the proposed recontruction of the river bed. Q=500m^3/s.

[4] Junk, W. J., P. B. Bayley and R. E. Sparks. The flood pulse concept in river-floodplain systems. *Canadian Special Publication in Fisheries and Aquatic Sciencies* **106**, 110–127, 1989.

[5] Roe, P.L., Approximate Riemann Solvers, Parameter Vectors and Difference Schemes *Journal of Computational Physics*, **43**, 357–372, 1981.

[6] Glaister P., Approximate Riemann solutions of the shallow water equations, *Journal of Hydraulic Research*, **26** (No.3), 293–306, 1988.

[7] Vreugdenhil C.B., *Numerical methods for shallow-water flow*. Kluwer Ac. Pub., Dordrecht, The Netherlands, 1994.

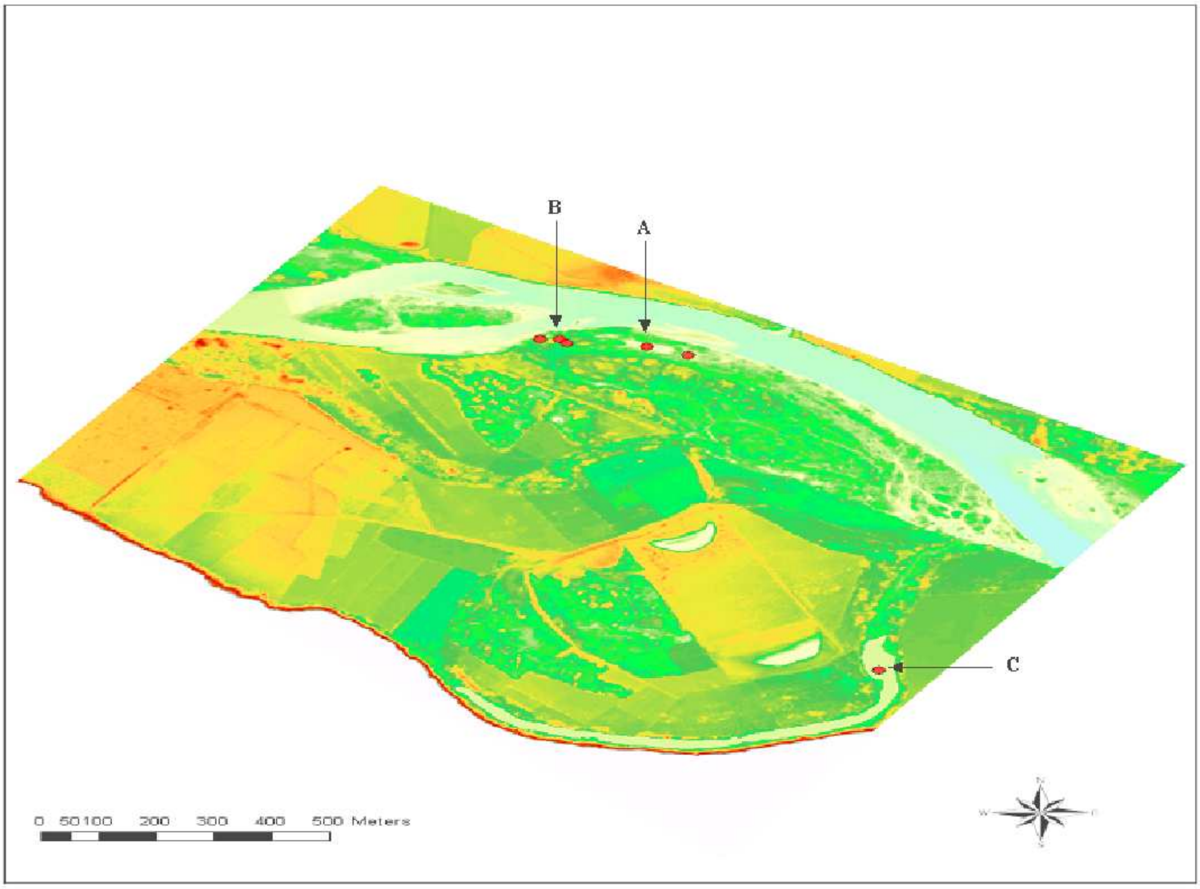

Figure 5: View of the river reach and location of three gauging points.

[8] Burguete J., Garcia-Navarro P., Efficient construction of high-resolution TVD conservative schemes for equations with source terms: application to shallow water flows, *International Journal for Numerical Methods in Fluids* **37**, 209–248, 2001.

[9] LeVeque R. J., Numerical methods for conservation laws, Birkhauser Basel, 1992.

[10] J. Murillo, P. García-Navarro, J. Burguete and P. Brufau. A conservative 2D model of inundation flow with solute transport over dry bed. *International Journal of Numerical Methods in Fluids* **52**, 1059–1092, 2005.

[11] Roe P.L., A Basis for Upwind Differencing of the Two-Dimensional Unsteady Euler Equations, *Num. Met. Fluid Dyn. II*, Oxford Univ. Press, 1986.

[12] Brufau P. and García-Navarro P., Two-dimensional dam break flow simulation, *Int. J. for Num. Meth. in Fluids*, **33** 35–57, 2000.

[13] Bermúdez, A., Dervieux P., Desideri J.A. and Vázquez M.E., Upwind schemes for the two-dimensional shallow water equations with variable depth using unstructured meshes, *Comput. Methods Appl. Mech. Engrg.*, **155** 49–72, 1998.

[14] Brufau P., Vazquez-Cendon M.E. and García-Navarro P., A numerical model for the flooding and drying of irregular domains, *Int. J. for Num. Meth. in Fluids*, **39** 247–275, 2002.

[15] Galat, D. L., L. H. Fredrickson, D. D. Humburg, K. J. Bataille, J. R. Bodie, J. Dohrenwend, G. T. Gelwicks, J. E. Havel, D. L. Helmers, J. B. Hooker, J. R. Jones, M. F. Knowlton, J. Kubisiak, J. Mazourek, A. C. McColpin, R. B. Renken, and R. D. Semlitsch, Flooding to restore connectivity of regulated, large-river wetlands - Natural and controlled flooding as complementary processes along the lower Missouri River. *Bioscience*, **48**, 721–733, 1998.

[16] H. M. Valett, M. A. Baker, J. A. Morrice, C. S. Crawford, M. C. Molles. Jr., C. N. Dahm, D. L. Moyer, J. R. Thibault and Lisa M. Ellis, Biogeochemical and metabolic responses to the flood pulse in a semiarid floodplain, *Ecology* **86** 220–234, 2005.

[17] Mayack, D. T., J. H. Thorp, and M. Cothran, Effects of burial and floodplain retention on stream processing of allochthonous litter, *Oikos* **54**, 378–388, 1989.

[18] Metzger, J. P., and H. Décamps, The structural connectivity treshold an hypothesis in conservation biology at landscape scale, *Acta Oecologica* **18**, 1–12, 1997.

[19] Tockner, K., and J. A. Stanford, Riverine flood plains: present state and future trends, *Environmental Conservation* **29**, 308–330, 2002.

[20] Vazquez-Cendon M.E., Improved treatment of source terms in upwind schemes for the shallow water equations in channels with irregular geometry, *Journal of Computational Physics*, **148**, 1999.